

Hybrid polymer nanocomposites with tailored band gaps and UV absorption for advanced applications in optoelectronics and UV protection

C. M. Kavitha¹ | K. M. Eshwarappa¹  | M. P. Shilpa² |
 Shivakumar Jagadish Shetty² | S. C. Gurumurthy² | K. U. Kiran³ | Sachin Shet⁴

¹Radiation and Materials Physics Lab,
 Department of Studies in Physics, Davanagere
 University, Davanagere, Karnataka, India

²Nano and Functional Materials Lab (NFML),
 Department of Physics, Manipal Institute of
 Technology, Manipal Academy of Higher
 Education, Manipal, Karnataka, India

³Department of Electronics, Maharani's
 Science College for Women (Autonomous),
 Mysuru, Karnataka, India

⁴Manipal Centre for Natural Sciences, Manipal
 Academy of Higher Education, Manipal,
 Karnataka, India

Correspondence

K. M. Eshwarappa, Radiation and Materials
 Physics Lab, Department of Studies in Physics,
 Davanagere University, Shivagangotri,
 Davanagere 577007, Karnataka, India.

Email: km.eshwarpappa@gmail.com

S. C. Gurumurthy, Nano and Functional
 Materials Lab (NFML), Department of Physics,
 Manipal Institute of Technology, Manipal
 Academy of Higher Education, Manipal
 576104, Karnataka, India.

Email: gurumurthy.sc@manipal.edu

Abstract

Herein we report the method to tailor the band gap and UV absorption of polyvinyl alcohol (PVA)/graphene oxide (GO)-silver (Ag)/glutaraldehyde (GA) hybrid polymer nanocomposites. The modifications brought by neutron irradiation to the optical and dielectric characteristics enabled the band gap and UV absorption-tailored polymer nanocomposites to be obtained. Neutron-irradiated samples, compared with their unirradiated counterparts, exhibit a reduction in transmittance to 78%, rendering them opaque to UV-visible light after irradiation. The energy band gap decreases from 5.25 to 4.09 eV upon irradiation. Furthermore, upon neutron-irradiation the relaxation time increases from 7.63×10^{-4} to 0.02 s which is evident by the shift in electric modulus imaginary part (M'') peak to a lower frequency region, indicating an increase in relaxation time. The Cole-Cole plot for irradiated samples demonstrates lower fitting parameter (α) values of the modified Havriliak-Negami function, indicating a departure from pure capacitor-like behavior. The neutron irradiation leads to a decrease in conductivity from 44.6×10^{-7} to 0.09×10^{-7} S/cm.

KEY WORDS

electric modulus, hybrid polymer nanocomposites, neutron, relaxation time, UV shielding

1 | INTRODUCTION

Polymer nanocomposites (NCs), which integrate a polymer matrix with various nanomaterials, demonstrate exceptional optical, electrical, thermal, and mechanical characteristics, making them essential as insulating material in power equipment function as dielectrics, providing mechanical support and high-voltage insulation, UV shielding, and electronic components such as power tool handles, cables, capacitors, packaging materials, industrial radiology, and nuclear waste handling.^{1–6} Undergoing radiation, especially harsh electromagnetic

radiation, neutrons, and rapid heavy ions, can induce changes in polymers. The extent of these changes depends on factors such as radiation type, energy, and flux. In applications like electronics, space research, medicine, dosimeters, and radiometry, specially developed polymers exhibiting specific responses to radiation are essential.^{7,8}

Interactions with non-ionizing radiation, particularly neutrons, are intriguing due to their unique influence on material atoms. Unlike other forms of radiation, neutrons lack a charge but have a mass equivalent to protons, allowing them to interact primarily with nuclei as they traverse a material. This interaction can lead to various effects,

This is an open access article under the terms of the [Creative Commons Attribution-NonCommercial-NoDerivs](#) License, which permits use and distribution in any medium, provided the original work is properly cited, the use is non-commercial and no modifications or adaptations are made.

© 2024 The Author(s). *Polymers for Advanced Technologies* published by John Wiley & Sons Ltd.

including deflection with or without energy loss and absorption by the material's nucleus.^{9,10} Exposure to high neutron fluence causes numerous defects in materials, leading to changes in physical properties. These changes include swelling, mechanical strength degradation, altered corrosion resistance, and modifications in optical, electrical, and thermal conductivity.¹¹

When neutrons transfer energy to the nuclei, it causes the displacement of atoms within polymeric chains, resulting in secondary knock-on effects and cluster formation. Charge transfer reactions can create ion clusters, which may lead to chemical breakdown upon neutralization. These interactions, especially nuclear recoils and transmutations, contribute significantly to radiation damage by disrupting the material's chemical structure.¹²⁻¹⁴ Fast neutrons primarily interact with protons in organic materials, generating recoil protons that induce chemical effects similar to those of high-energy protons.^{15,16}

Incorporating nanomaterials into polymer matrices has been shown to significantly modify their properties, particularly in radiation environments. For example, Abdelmalik et al. suggested that adding 1 wt% TiO₂ nanoparticles (NPs) to an epoxy polymer can enhance its dielectric and polarization relaxation behavior, thereby improving resistance to radiation-induced degradation in nuclear environments.¹⁷ Additionally, Abdelmalik highlighted that lower dielectric loss was observed in NC systems with 2 wt% NP loading, possibly due to hindrances in charge transport through various chains and interfaces.¹⁸ Upon neutron exposure, Shilpa et al. found that the ionic conductivity significantly increased for Ag-incorporated polyvinyl alcohol (PVA)-NaBr.¹⁹ Yang et al. emphasized the importance of regional carrier migration and dipole polarization in the polarization process of epoxy resin NCs, suggesting that these factors play a dominant role in enhancing the material's properties.²⁰

Polymer NCs offer radiation resistance and are effective in shielding neutrons as these materials are composed of mainly low-atomic number elements. Galehdari's findings demonstrated increased neutron shielding efficiency in epoxy NCs compared with neat epoxy, indicating their potential for improved radiation shielding applications.²¹ Canel et al. highlighted the superior shielding properties of metal powder-filled epoxy composites for neutron-gamma mixed fields, with TiO₂-filled epoxy composites being particularly effective.²² Limin Jiao et al. demonstrated that incorporating hexagonal boron nitride (h-BN) into epoxy resin significantly improves radiation resistance and neutron shielding, a benefit that could extend to other polymer materials as well.²³ Basha further reported that Polyvinylpyrrolidone (PVP) Fourier /gelatin blends doped with dysprosium (III) chloride could serve as good candidate for dosimeters.⁸ Moreover, Abuali Galehdari's work indicated an increased elastic modulus in non-irradiated NCs, suggesting that these materials could be advantageous for neutron shielding structures due to their enhanced mechanical properties.²¹

Neutron irradiation can bring heat resistance to the polymer NC. Behmanesh et al., thermogravimetric analysis (TGA) revealed that the heat resistance of PVA/Ag₂O composite varies with different doses of gamma and neutron irradiation, highlighting the complex interactions between radiation and polymer composites.²⁴ The above studies collectively suggest that the integration of nanomaterials such as TiO₂, h-BN, Ag₂O, and metal powders into polymer matrices like

epoxy and PVA can significantly enhance their dielectric, mechanical, and shielding properties, particularly in radiation environments. Such advancements underscore the potential of these NCs for applications requiring tailoring the properties for robust performance.

It can be noticed from the above that the majority of research has focused on the use of polymer NCs for radiation shielding, but very less effort directed toward understanding the effects of neutron radiation on their properties. Since the neutron interactions can lead to changes in the properties of materials hence offers the possibility of tuning the properties of polymer NCs. To the best of our knowledge limited literature is available on using neutron radiation for tailoring the properties of materials, particularly polymer NCs may be due to the lack of availability of a neutron source. To exploit the potentiality of neutron irradiation and to address the existing gap, the current study explores the synthesis (using a straightforward *in situ* method), characterization, and neutron radiation effects on PVA/graphene oxide (GO)-silver (Ag)/glutaraldehyde (GA) NCs. By investigating neutron-induced modifications, we aim to elucidate how these interactions affect the optical and electrical properties of the material. The novelty of this approach lies in the precise examination of the combined effects of neutron irradiation and cross-linking agent GA within the PVA/GO-Ag/GA composite, offering insights into developing high-performance nanoenergy devices and flexible electronic applications.

2 | EXPERIMENTAL DETAILS

The PVA-GO-Ag/GA film was prepared by sonicating 0.5 wt% GO in 20 mL deionized water for an hour. 1.2 g of PVA was dissolved in 20 mL water with heating and stirring until transparent, then combined with the GO solution and stirred at 50°C for an hour. Followed by addition of 0.1 wt% AgNO₃ and 2 mL (1 vol%) GA and heated for another hour. The films were then neutron-irradiated.

Details of the synthesis and fabrication of PVA/GO-Ag/GA films can be found in our earlier paper.²⁵

2.1 | Neutron source and its specifications

Americium-Beryllium (AmBe) neutron source available at Manipal Centre for Natural Sciences, Manipal Academy of Higher Education, Manipal, Karnataka has been employed for neutron irradiation.

Specifications:

Source strength: 16 Ci

Irradiation channel dimension: 40 cm × 40 cm × 70 cm.

Neutron flux: 5×10^3 neutrons $\text{cm}^{-2} \text{s}^{-1}$ at 10 cm from source

Dose rate at the irradiation location: 12 mSv/h

2.2 | Neutron irradiation studies

The prepared samples of dimensions 3 cm × 3 cm were subjected to neutron irradiation. The samples were placed 10 cm away from a 16 Ci

AmBe neutron source housed within a concrete bunker featuring a specialized irradiation channel measuring 40 cm × 40 cm × 70 cm. The neutrons emitted from this neutron source are of a broad energy spectrum. The neutron flux from the source was estimated to be approximately 5×10^3 neutrons $\text{cm}^{-2} \text{ s}^{-1}$ at a distance of 10 cm, and the dose rate at the irradiation location was found to be 12 mSv/h. The samples underwent irradiation at varied intervals of time, and the corresponding neutron fluence values were calculated and presented in Table 1. Schematic diagram of neutron irradiation is illustrated in Scheme 1.

3 | RESULTS AND ANALYSIS

3.1 | Morphological examination

The morphology of unirradiated and neutron-irradiated PVA/GO-Ag/GA NC films obtained utilizing a scanning electron microscope (SEM)

TABLE 1 Sample description with time integrated neutron flux.

Samples	Fluence (n/cm^2)	Sample code
PVA	0	S0
PVA/GO-Ag/GA	0	S1
	6.48×10^9	S2
	1.04×10^{10}	S3
	1.60×10^{10}	S4
	4.19×10^{10}	S5

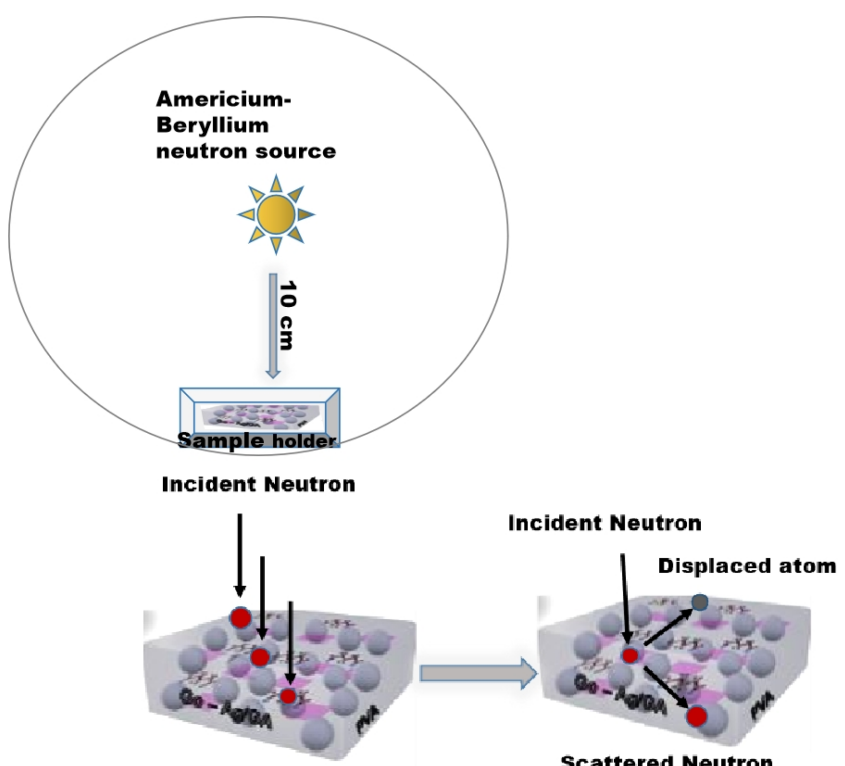
Abbreviations: Ag, silver; GA, glutaraldehyde; GO, graphene oxide; PVA, polyvinyl alcohol.

is depicted in Figure 1. In the case of PVA (Figure 1A), the surface is uniform with minimal surface roughness. Upon the incorporation of nanofillers, as illustrated in Figure 1B, surface irregularities are observed due to the presence of GO, accompanied by white spots indicating the formation of Ag NPs. The impact of neutron irradiation on these NC films is evident in morphological changes. Neutron irradiation induces holes on the surface of the S2 film, as seen in Figure 1C, compared with the S1 film (Figure 1B).

Furthermore, there is a noticeable reduction in the number of Ag NPs, which is evident by elemental composition values detailed in Table 2. This is because, neutron irradiation can lead to the coalescence of smaller particles into larger aggregates due to increased atomic mobility and diffusion under irradiation conditions. This results in a decrease in the number of discrete NPs, even though the total mass of silver remains constant. These morphological changes are in line with the Farag et al.²⁶ observations. With an increase in neutron fluence (S5), the holes on the film's surface decrease, coupled with folds of GO layers and Ag NPs exhibiting agglomeration (Figure 1D).

3.2 | Fourier Transform Infrared (FTIR) analysis

FTIR investigations were conducted to examine alterations in the structure of polymers resulting from the inclusion of fillers and upon neutron irradiation, as depicted in Figure 2A. In S0, the presence of functional group OH is evident through a prominent absorption peak at 3299 cm^{-1} , while the peak corresponding to asymmetric and symmetric stretching vibration of $-\text{CH}_2$ groups is appearing at 2923 cm^{-1} . Peaks corresponding to the stretching modes of C=O



SCHEME 1 Schematic illustration of neutron irradiation on PVA/GO-Ag/GA nanocomposite. Ag, silver; GA, glutaraldehyde; GO, graphene oxide; PVA, polyvinyl alcohol.

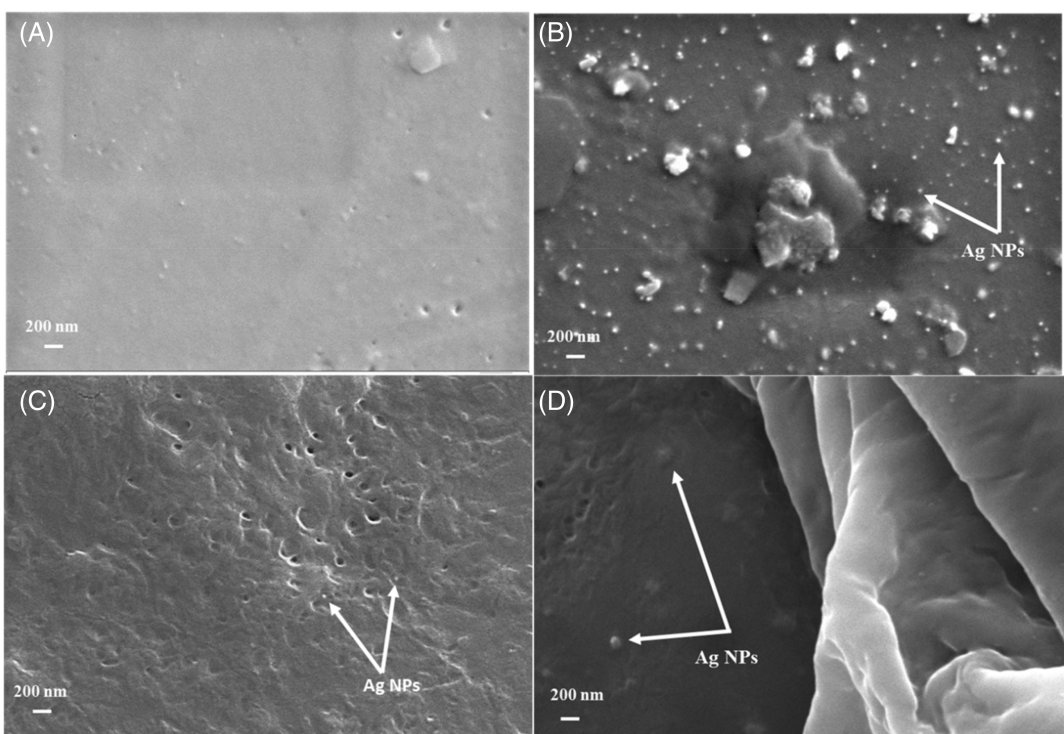


FIGURE 1 The surface structure of (A) unirradiated PVA. PVA/GO-Ag/GA films under neutron fluence: (B) 0 n/cm² fluence, (C) 6.48 × 10⁹ n/cm² fluence, and (D) 4.19 × 10¹⁰ n/cm² fluence. Ag, silver; GA, glutaraldehyde; GO, graphene oxide; NPs, nanoparticles; PVA, polyvinyl alcohol.

TABLE 2 Energy Dispersive X-Ray Analysis (EDXA) results of fabricated polymer nanocomposites.

Sample	Elements		
	Carbon wt %	Oxygen wt %	Silver wt %
S0	54.92	45.08	-
S1	55.01	44.01	0.99
S2	54.80	44.61	0.59
S5	53.25	45.73	1.02

bonds are observed at 1718 cm⁻¹ respectively. However, the bands due to bending and wagging vibrations of the CH₂ groups appear at 1419 and 1366 cm⁻¹, while acetal linkage (—C—O—C—) stretching vibrations appeared at 1079 cm⁻¹.

GA acts as a cross-linking agent by forming covalent bonds with the hydroxyl groups present in the PVA polymer matrix as depicted in Scheme 2. The aldehyde groups of GA are highly reactive and can form Schiff base linkages (R—CH=N—R') with the hydroxyl groups of PVA effectively creating a network of covalently bonded polymer chains.

Our earlier work²⁷ on the mechanical properties such as tensile strength and elongation at break can indicate the cross-linking

efficiency. Higher tensile strength and lower elongation at break are typical of highly cross-linked polymers. The reduction in the —OH and C=O peak intensities, coupled with the appearance and increase in the C=N peak intensity, can provide a measure of the cross-linking efficiency.

The degree of cross-linking (DC) can be estimated using the ratio of the integrated areas under the corresponding FTIR spectra peaks, that is

$$DC = \frac{A_{C=N}}{A_{OH} + A_{C=O} + A_{C=N}}$$

where A_{C=N} is the area under the C=N peak, A_{OH} is the area under the OH peak, and A_{C=O} is the area under the C=O peak. A DC was 0.33 indicating a moderate level of cross-linking suggests one-third of the functional groups in the PVA matrix are involved in cross-linking, leading to significant changes in the material's properties.^{28,29}

In S1 (Figure 2A), it can be seen that the narrowing and reduction of the OH peak compared with S0 indicate a reduced concentration of the OH group. Due to the strong interaction between PVA with GO and Ag NPs, a shift in the peak from 3299 to 3493 cm⁻¹ was observed. The peak attributed to the C—O—C stretching shifted to higher frequencies. This shift occurred because of the formation of bound C—O—C bonds in acetal and ether linkages, resulting from the reaction between hydroxyl groups and the cross-linker, GA. The interactions including, the bonding between PVA and GO, the stabilization

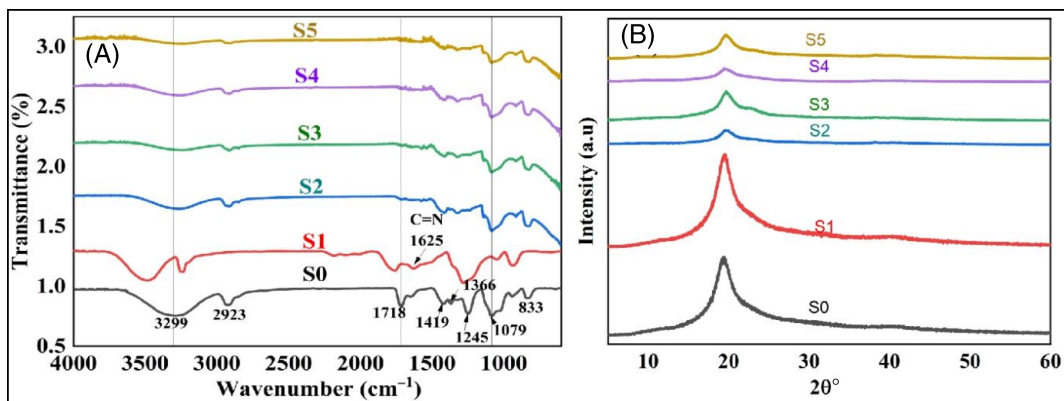
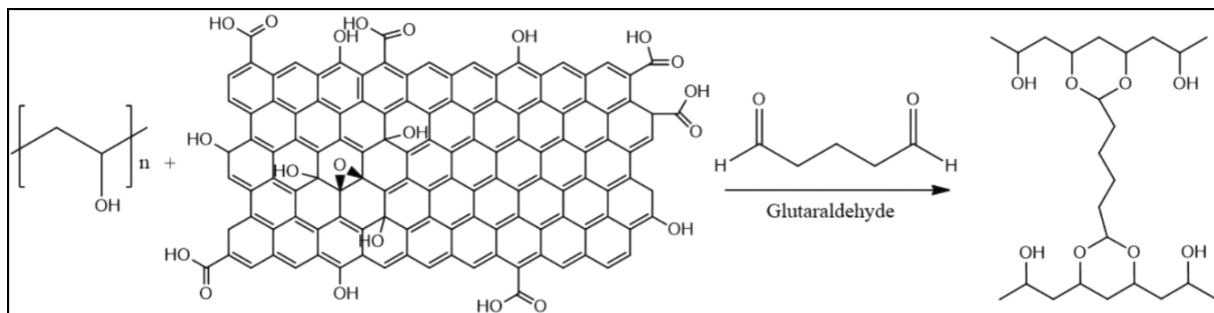


FIGURE 2 The characterization of polymer nanocomposites, with (A) presenting the FTIR spectra and (B) illustrating the X-Ray Diffraction (XRD) spectra of samples designated as S0, S1, S2, S3, S4, and S5. These spectra depict the structural and crystalline alterations resulting from the integration of fillers and neutron irradiation.



SCHEME 2 A Schematic representation of cross-linking formation between GA, PVA, and GO. GA, glutaraldehyde; GO, graphene oxide; PVA, polyvinyl alcohol.

effects of Ag NPs, and the cross-linking facilitated by GA would be inferred from the disappearance of the bands at 1419 and 1366 cm^{-1} . This signifies the completion of cross-linking reactions where functional groups are consumed.³⁰ The reduction in the $-\text{OH}$ and $\text{C}=\text{O}$ peak intensities, coupled with the appearance and increase in the $\text{C}=\text{N}$ peak intensity, A DC was 0.33 indicating that one-third of the functional groups in the PVA matrix are involved in cross-linking, leading to significant changes in the material's properties. This value represents a moderate level of cross-linking. Our earlier work^{2,31} has extensively covered the analysis of functional groups in PVA and PVA/GO-Ag/GA.

Polymer NCs exposed to neutron radiation (S2, S3, S4, and S5) a disappearance of the intensity of bands within the 1770–1650 cm^{-1} range was observed. Neutron irradiation can break down carbonyl groups and cause cross-linking reactions that consume these groups. This process forms new bonds, resulting in peaks at 1429 and 1330 cm^{-1} , corresponding to CH_2 bending and wagging vibrations. Additionally, interaction with metal NPs or other components in the NC under irradiation can further alter the carbonyl groups, leading to the disappearance of their characteristic IR bands. This loss of functional group suggests the evaporation of water molecules, initially trapped within the polymer matrix during the synthesis or processing of the composite, are released upon irradiation or under specific

TABLE 3 Values for the crystallite size (D) and crystallinity index (X_c) calculated using XRD data: the combined area of the amorphous and crystalline peaks (x_c+x_a) and the total area of the crystalline peaks (x_c).

Samples	(x_c)	(x_c+x_a)	$X_c = \frac{x_c}{(x_c+x_a)}$	$D = \frac{K\alpha}{\beta \cos\theta} (\text{nm})$
S0	22522.97	34707.39	44.21	9.26
S1	15344.40	37926.31	40.46	4.58
S2	9854.97	21051.41	46.81	2.89
S3	17684.3	27493.72	64.32	3.06
S4	16387.08	27576.66	59.42	3.17
S5	12188.5	26362.53	46.23	3.43

environmental conditions in the polymer matrix due to neutron irradiation. The OH peak at 3493 cm^{-1} shifted to 3266 cm^{-1} in the irradiated sample and weaken after neutron irradiation, which is attributed to a decrease in the concentration of OH groups as a result of the breaking of OH groups. Further, it can be seen from Table 3 that there is an increase in the crystallinity index, indicating that OH groups in PVA may participate in cross-linking reactions, forming new chemical bonds and reducing the OH group concentration. Moreover, with increased fluence, the peaks in the 1200–1500 cm^{-1} region

diminished, indicating bond scission leading to fragmentation of molecular structure and also removal of these groups which lead to diminished peak intensity. It can be noticed from Figure 2A that an increase in fluence up to $1.04 \times 10^{11} \text{ n/cm}^2$ decreases all peak intensities, but for the fluence of $1.60 \times 10^{11} \text{ n/cm}^2$ peak intensity of all peaks increases. Further, the increase in the fluence to $4.19 \times 10^{11} \text{ n/cm}^2$ peak intensity of all peaks decreases. At lower fluence, defect creation dominates, reducing peak intensities. At intermediate fluencies, some defect recombination or reorganization can

increase peak intensities. At higher fluence, extensive damage and disorder dominate, leading to a significant reduction in peak intensities.

3.3 | XRD analysis

XRD pattern as depicted in Figure 2B reveals the crystalline and amorphous phases of unirradiated pure PVA. In addition, distinct crystalline peaks of S0 at $2\theta = 19.47^\circ$ (101) (Figure 3A) in S1 increase with filler

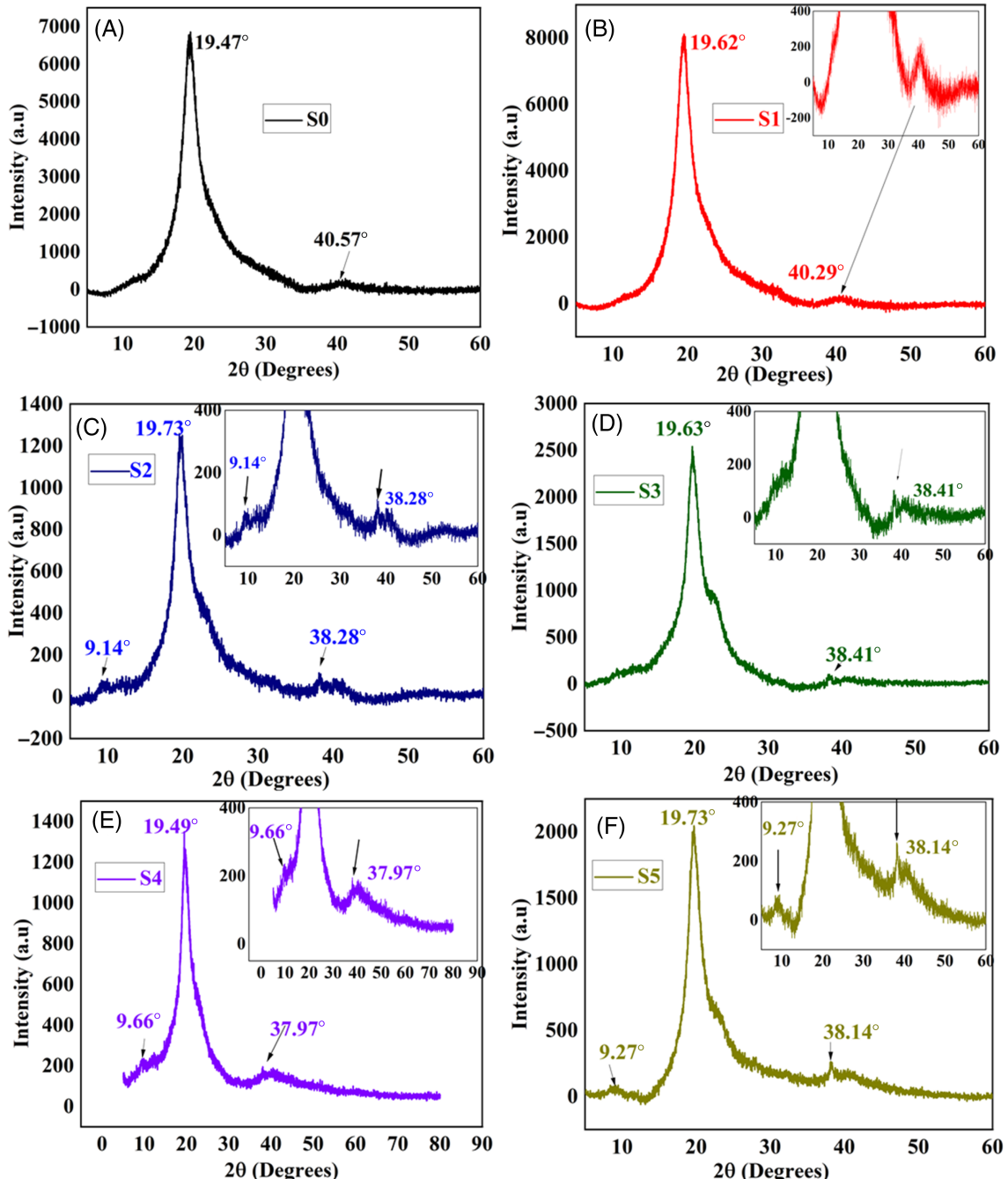


FIGURE 3 XRD spectra of (A) unirradiated PVA. XRD spectra of PVA/GO-Ag/GA (B) 0 n/cm^2 fluence, (C) 6.48×10^{10} , (D) 1.04×10^{11} , (E) 1.60×10^{11} , and (F) $4.19 \times 10^{11} \text{ n/cm}^2$. Ag, silver; GA, glutaraldehyde; GO, graphene oxide; PVA, polyvinyl alcohol.

incorporation, indicating increased crystallinity (Table 3). Additionally, a peak shift towards a higher 2θ value is observed, confirming the presence of filler crystallites within the polymeric matrix.³² Notably, as mentioned in our earlier work,³¹ no discernible peaks regarding fillers are visible (Figure 3B), suggesting the masking effect of the PVA matrix or the peak is too weak to be detected.

As revealed by Figure 3C, upon irradiation with fast neutrons at a fluence of $6.48 \times 10^9 \text{ cm}^{-2}$, the diminished peak corresponding to PVA indicates structural variations in the polymeric network of NCs. Furthermore, one can notice the appearance of new peaks at $2\theta = 9.34^\circ$ (GO)³³ and 38.28° (Ag)³⁴ due to the enhanced orderly arrangement of GO and Ag as a result of neutron irradiation. This might also be due to decrease in the crystallinity of the polymeric matrix, enhancing the crystallite structure of fillers and enabling them to produce diffraction peaks.

However, for S3, the intensity of the PVA peak (Figure 3D) increases slightly compared with S2, indicating a rise in crystallinity (Table 3) within the PVA matrix due to cross-linking. This leads to increased filler dispersion, reducing the structural orderliness of the filler, resulting in the nearly disappearing GO peak and decreased Ag peak intensity. Moreover, further increase in fluence to $1.60 \times 10^{10} \text{ n/cm}^2$ (S4) and $4.19 \times 10^{10} \text{ n/cm}^2$ (S5), the XRD peak intensities of GO and Ag NPs appear prominently (Figure 3E,F) due to the decrease in crystallinity of polymer NC as evident in Table 3. At higher fluence, neutron irradiation may promote the agglomeration or clustering of Ag NPs. This aggregation results in larger crystalline domains, leading to more intense XRD peaks. Neutron radiation can also affect the concentration and distribution of functional groups on the surface of GO. Changes in the concentration of these groups can influence the interaction between NPs and their surroundings, affecting the XRD peak intensities of fillers.

3.4 | Optical analysis

Neutron irradiation prompts a peak shift towards shorter or longer wavelengths. This is because neutron irradiation creates or annihilates defects

in the material's crystal lattice, introducing energy levels within the band structure depending upon the neutron fluence. Further, chemical reactions triggered by neutron irradiation might result in changes to the material's electronic structure or molecular configurations. In tandem, UV-vis spectroscopy Figure 4 unveils electronic transitions in molecules. For polymer NCs (S0–S5), in Figure 4A the addition of fillers and GA induces absorbance, particularly a plasmonic peak at 441 nm for S1, and 431 nm for S2 showing an increase in peak intensity which reflects the formation of more defects after neutron irradiation and introduces new energy levels at near to top of the conduction band. For further increase in fluence to $1.04 \times 10^{11} \text{ n/cm}^2$ (S3) and $1.60 \times 10^{11} \text{ n/cm}^2$ (S4) the plasmon peak further shifts to 429 and 426 nm respectively with a decrease in intensity which might be due to introduction of new energy levels far from the top of the conduction band. Finally for the neutron fluence of $4.19 \times 10^{11} \text{ n/cm}^2$ (S5) plasmon peak shifts to 435 nm with an increase in intensity which can be attributed to the annihilation of the most energy levels which are far from top of the conduction band.

The light transmittance in Figure 4B plots reveal that S0 exhibits the highest light transmittance at 86%, while the unirradiated PVA/GO-Ag/GA film has a transmittance of 42%, this amounts to decrease in the transmittance of S1 by 51% compared with S0. However, for all irradiated films, transmittance drops below 10% which is equal to reduction by 78% compared with S1, rendering them opaque to UV-visible light after damage. However, the transmittance increases slightly beyond 450 nm region. This reduction in transmittance, especially in the UV range, indicates potential applications in UV-blocking, making these films suitable for scenarios requiring enhanced protection against harmful UV radiation, such as in UV shielding coatings or packaging materials.

3.4.1 | Energy band gap

The energy gap (E_g) can be determined using the following formula^{17,35}:

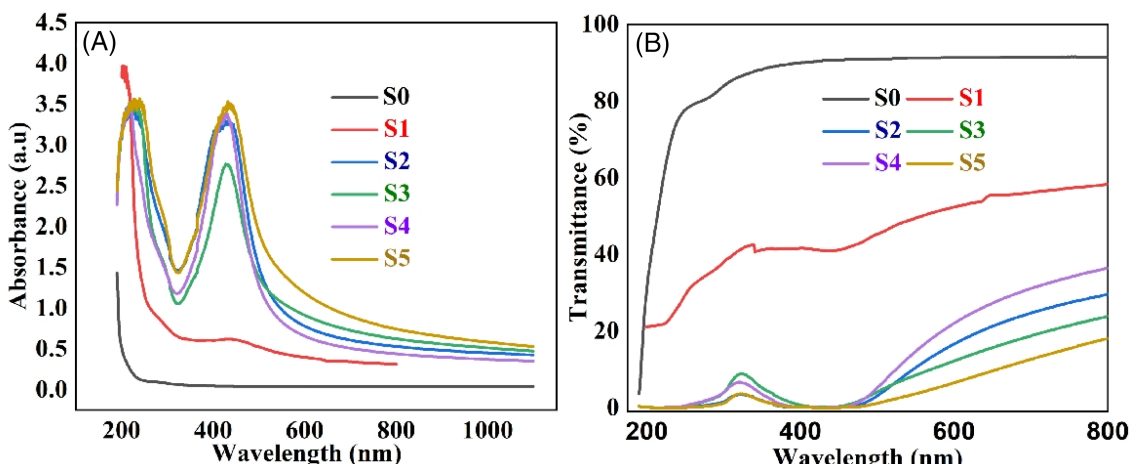


FIGURE 4 (A) Absorbance spectra of polymer nanocomposites (S0, S1, S2, S3, S4, and S5), showcasing variations in absorbance and providing insights into the optical properties of the nanocomposite materials. (B) Transmittance spectra of polymer nanocomposites (S0, S1, S2, S3, S4, and S5), highlighting variations in transmittance and offering valuable information on the optical characteristics of the nanocomposite materials.

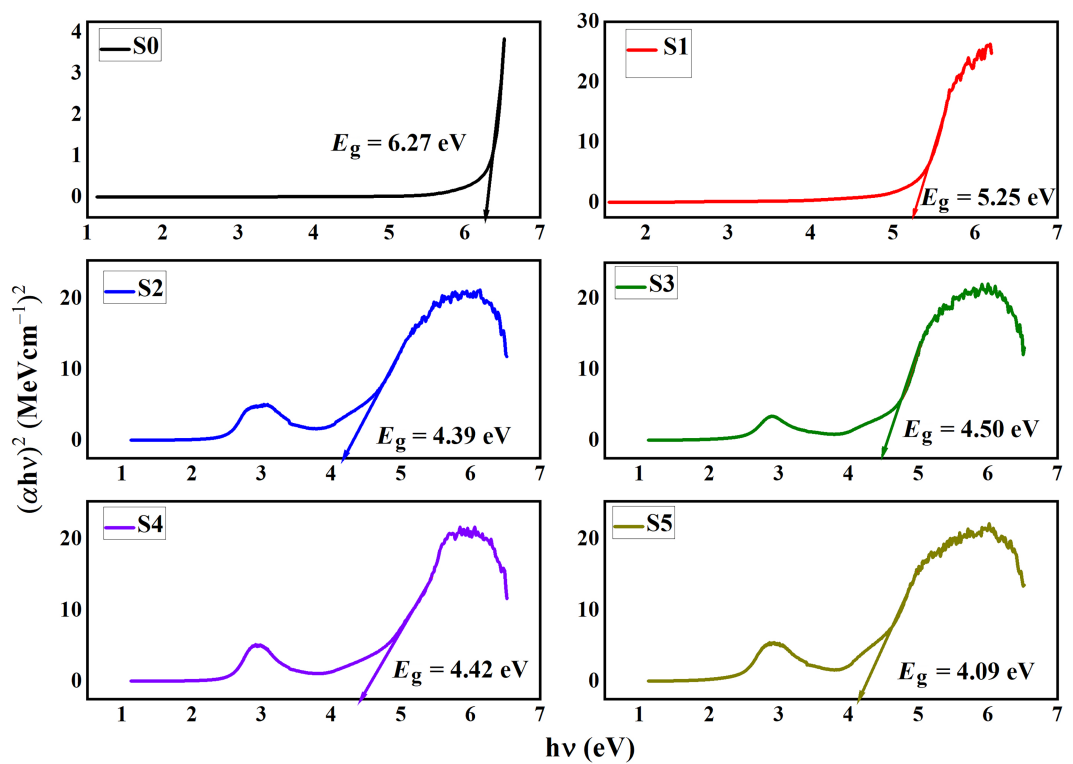


FIGURE 5 Illustration of the effect of neutron exposure on PVA and PVA/GO-Ag/GA polymer nanocomposite's optical band gap determined using Tauc's method. Ag, silver; GA, glutaraldehyde; GO, graphene oxide; PVA, polyvinyl alcohol.

$$\alpha h\nu = A(h\nu - E_g)^s, \quad (1)$$

where, A is the quality factor associated with transition probability, $h\nu$ is the photon energy, α is the absorption coefficient, and s is linked to the prevailing electronic transition for direct-allowed, direct-forbidden, indirect-allowed, or indirect-forbidden transitions, which takes values of $1/2$, $3/2$, 2 , or 3 , respectively. The E_g , is obtained by the linear intersection of the curve with the x-axis of the plot $(\alpha h\nu)^2$ versus $h\nu$, with A representing the slope of the straight line.

In Figure 5, the band gap energies of both unirradiated and neutron exposed polymer NCs are illustrated. With the introduction of fillers, there is a noticeable reduction in the band gap energy from S0 to S1, decreasing from 6.27 to 5.25 eV. Upon irradiation, the E_g value initially decreases to 4.39 eV, indicating a fall in the resistivity of the polymer NCs. The observed reduction is associated with the structural impairment of GO and Ag NPs, contributing to fragmentation and defect formation.

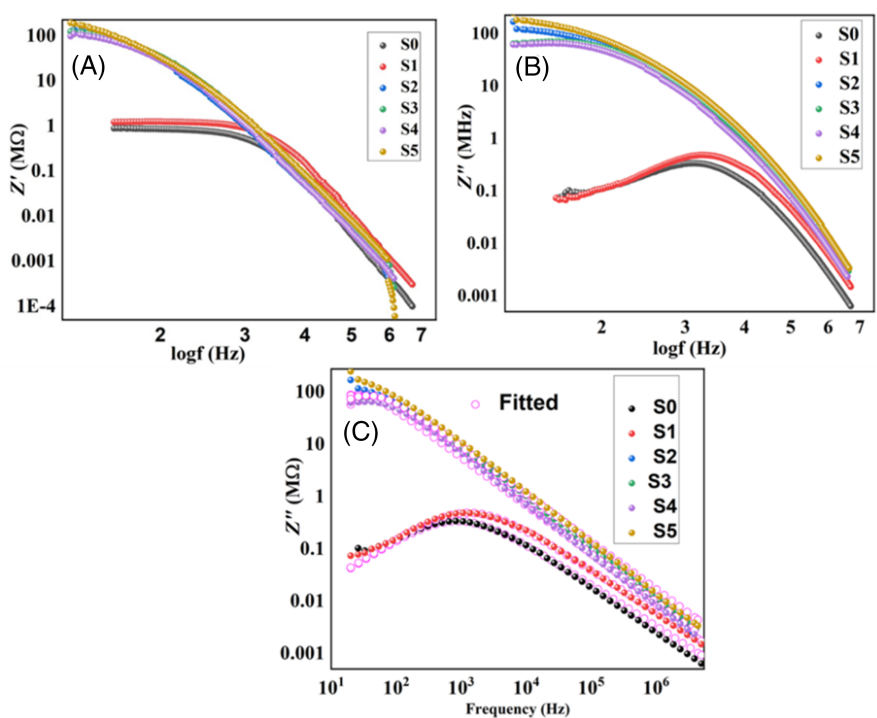
This structural damage induces degradation in crystallinity, size, and overall properties. Ag NPs agglomerate due to polymer chain mobility generated by neutron irradiation. Additionally, this process also leads to the formation of new energy levels as a result of neutron exposure. Notably, for S3, there is an increase in the E_g value to 4.50 eV. This phenomenon is ascribed to the reversion of atoms in the outermost crystallite zones, which were previously dispersed, back to their original lattice positions.¹⁴ Moreover, the metallic atoms already in a reduced state act as preorganized seed points, catalyzing

the direct growth of silver NPs on the polymer backbone. Progressing from S3 to S5, a consistent reduction in the E_g value is evident ultimately reaching 4.09 eV with increasing neutron fluence.

3.5 | Impedance analysis

Impedance analysis proves valuable in distinguishing between the effects of grain boundaries and grain electrodes, particularly concerning oxygen vacancies and other defects within the material. This analytical approach aids in identifying space charge polarization and its relaxation mechanisms by assigning specific capacitance and resistance values to both the grain and grain boundary effects.³⁶ Real impedance (Z') represents the ability of the material to resist the flow of electrical current in the circuit whereas, imaginary impedance (Z'') depicts the ability of a material to store electrical energy.³⁷ Figure 6 shows the Z' and Z'' plots versus log frequency for irradiated and unirradiated samples. The low-frequency range shows an increase in the Z' and Z'' of both PVA and PVA/GO-Ag/GA. Higher Z' values indicate larger electrode polarization at lower frequencies. The increase in the Z'' at lower frequencies is often associated with processes related to charge accumulation or redistribution within the material. Figure 6A shows an increase in impedance for S1 compared with S0 after NP incorporation. This increase suggests a reduction in orientation polarization due to strong bonding between polymer chains and NP surfaces.

FIGURE 6 The plot of (A) real part of impedance against log frequency, (B) imaginary part of impedance against log frequency, (C) Z'' versus frequency of neutron irradiated samples and additionally shown in (C) are the outcomes fit to modified Havriliak-Negami function.



All samples exhibited increased impedance upon neutron irradiation, with the magnitude of Z' increasing at lower frequencies. This is attributed to free radicals generated during irradiation might have reacted with NPs, modifying dipolar groups and reducing mobile charge carriers in the polymer matrix, contributing to the observed increase in impedance.¹⁷ However this is dose-dependent, at higher doses (S4), the fragmentation of the polymer chain leads to the free movement of nanofillers, and also increased space charge accumulation may have reduced the reaction of free radicals with NPs, thereby increasing the mobile charge carriers and subsequently reducing the impedance. However, with a further increase in fluence ($4.19 \times 10^{10} \text{ n/cm}^{-2}$), Z' increased, indicating decreased degradation likely due to cross-linking, which hinders the mobility of charge carriers and consequently increases the impedance.

Figure 6B depicts the frequency dependence of the imaginary part (Z'') of impedance with respect to fluence. Peaks with asymmetric broadening for S0 and S1 suggest relaxation in the materials attributed to grain boundaries.³⁸ Subsequently, at lower frequency regions, Z'' increases drastically for irradiated samples, indicating an enhancement in the resistive property. Furthermore, it is evident that the peaks are beyond the scale, indicating a shift towards the lower frequency region, typically suggesting an increase in the relaxation time of the material. This shift implies that the material takes longer to respond to the applied alternating current (ac) signal. From Figure 6 it is seen that Z'' is fluence-dependent, initially, at lower fluence levels, the Z'' (S2 and S3) was high, indicating a strong resistive property in the material. As the fluence increased to 1.60×10^{10} (S4), Z'' decreased, suggesting a reduction in the resistive behavior. This decrease could be attributed to various factors, such as changes in the material's structure or the interaction between radiation and the NCs.

However, with further increases in fluence 4.19×10^{10} (S5), Z'' increases again. This reversal in behavior might occur due to additional radiation-induced processes, such as the formation of new defects or the activation of different mechanisms within the material, leading to increased resistive properties. It can be noticed that the same trend is observed in FTIR analysis.

In frequency domain analysis, the Havriliak-Negami (HN) empirical function is a commonly employed method for data characterization. The HN function fitting results provide a quantitative measure of the relaxation dynamics in the NC. By analyzing these results, we can infer the impact of neutron irradiation on the material's structure and electrical properties. The HN function fitting is expressed as follows³⁹:

$$F_{\text{HN}}(\omega) = \frac{1}{[1 + (i\omega\tau_{\text{HN}})^{\alpha\beta}]}, \quad (2)$$

where α and β are the shape parameters and it is easier to determine the resonance frequency (f_c), aligned with the peak value of Z_{max} , by utilizing the imaginary component of impedance. This frequency can be expressed as $c = \frac{1}{2\pi\tau} = \frac{1}{2\pi RC}$, where $\tau = RC$ represents the critical relaxation time. Additionally, α serves as the fitting parameter, and the critical frequency is denoted by $\omega_c = 1/\tau$. An α value of 1 signifies a Debye-type relaxation mechanism, and the range of α values spans from 0 to 1 signifying non-Debye type. Figure 6C presents the HN function fitting of the experimental data, highlighting the effect of neutron fluence on the frequency-dependent behavior of the imaginary part of complex impedance. The computed values are detailed in Table 4. However, for all samples, the α values were less than 1, signifying the absence of a Debye-type mechanism. In contrast, the β value

Samples	α	β	τ (s)
S0 (PVA)	0.79 ± 0.99	1.00 ± 0.15	$1.14 \times 10^{-3} \pm 7.89 \times 10^{-5}$
PVA/GO-Ag/GA	S1	0.80 ± 0.02	1.00 ± 0.03
	S2	0.98 ± 0.02	0.97 ± 0.01
	S3	0.97 ± 0.06	0.96 ± 0.02
	S4	0.98 ± 0.08	0.95 ± 0.02
	S5	0.93 ± 0.01	0.98 ± 0.01
Note: These values, derived from the observations in Figure 6C.			

Abbreviations: Ag, silver; GA, glutaraldehyde; GO, graphene oxide; HN, Havriliak-Negami; PVA, polyvinyl alcohol.

for S0 and S1 is found to be 1, while for all irradiated samples, it falls between 0 and 1.

The unirradiated sample exhibit lower α values compared with irradiated samples, hence shows narrow distribution of relaxation process. An increase in α after irradiation suggests that neutron exposure introduces more heterogeneity in the relaxation processes leading to broader distribution (Table 4), possibly due to the creation of free volume, defects, which change polymer chain mobility. The β parameter is related to the asymmetry of the relaxation peak. A β value of 1 for an unirradiated sample corresponds to a symmetric relaxation process, while values less than 1 upon irradiation indicate an asymmetric process, often associated with non-Debye relaxation behavior. A decrease in β increases asymmetry, possibly due to the interaction of neutron-induced defects with the polymer matrix.

The changes in relaxation dynamics also impact charge transport processes within the NC. Increased heterogeneity and asymmetry in relaxation disrupt the uniformity of charge transport pathways due to the creation of free radicals and ion clusters, indicating that charge carriers encounter more barriers and traps, leading to decreased conductivity as evidenced by Table 6.

3.5.1 | Nyquist or Cole–Cole plot

To arrive at the equivalent circuit the Electrochemical Impedance Spectroscopy (EIS) open-source spectrum analyzer software tool was utilized. The Z^* plots, encompassing the real and imaginary parts of the impedance, were accurately fitted for various neutron fluencies on PVA/GO-Ag/GA composites. The equivalent circuit, comprising capacitance (C) in series with the parallel combination of CPE1 and CPE2, was computed based on the Z^* plots.

Figure 7A depicts the complex impedance plots, showing a high-frequency semi-circle for S0 and S1. The fitted curves for S2, S3, S4, and S5 are illustrated in Figure 7B. The corresponding values for C, CPE1, and CPE2 are presented in Table 5. The constant phase element (CPE) arises from a distribution of time constants, attributed to the interface resistance (R) and/or interfacial capacitance (C). The impedance of a CPE is described by Equation (3).⁴⁰

TABLE 4 HN function fitting parameters: α , β , and τ .

$$Z_{\text{CPE}} = \frac{1}{(j\omega)^{\alpha} Q} \quad (3)$$

In the provided relation, Q and α are parameters defining the CPE. The parameter α is dimensionless and ranges between 0 and 1. When α equals 1, the system behaves as a pure capacitor. On the other hand, if α lies between 0.6 and 1, the impedance diagrams exhibit significant distortion, forming a straight line at a $(90 \times \alpha)^\circ$ angle with the x-axis in the Nyquist representation. For unirradiated samples (S0 and S1), α values lies close to 1 (Table 5) indicate a behavior approaching that of a pure capacitor, suggesting minimal distortion in the impedance diagrams. The corresponding Q values reveal a consistent distribution of time constants.

In contrast, irradiated samples (S2, S3, S4, and S5) exhibit lower α values, indicating a departure from a pure capacitor-like behavior. Additionally this decrease in α values further signifies changes in the distribution of time constants (Table 4). Also change in α suggests alterations in the charge transfer processes and impedance characteristics.

3.5.2 | Dielectric studies

A widely employed technique for elucidating the source of dielectric dispersion involves examining the real part of dielectric (ϵ') in polymeric materials. The complex permittivity of the material is expressed in Equation (4)

$$\epsilon^* = \epsilon' - j\epsilon'' \quad (4)$$

where $j = \sqrt{-1}$ and ϵ' and ϵ'' are real and imaginary parts of the complex permittivity respectively. Figure 8A illustrates the frequency-dependent behavior of ϵ' for both S0 and S1. Notably, the values of ϵ' decrease with the rising applied frequency. This variation in ϵ' is primarily attributed to space-charge polarization up to 104 Hz, with higher frequencies incorporating contributions from ionic, dipolar, and electronic polarization mechanisms.⁴¹ In Figure 8A, the introduction of nanofillers, specifically GO, Ag NPs, and GA as a cross-linking agent, significantly impacts the dielectric constant of the NC compared with pure PVA. The combined effect of GO, Ag, and GA results in a complex interaction that influences the dielectric constant. While

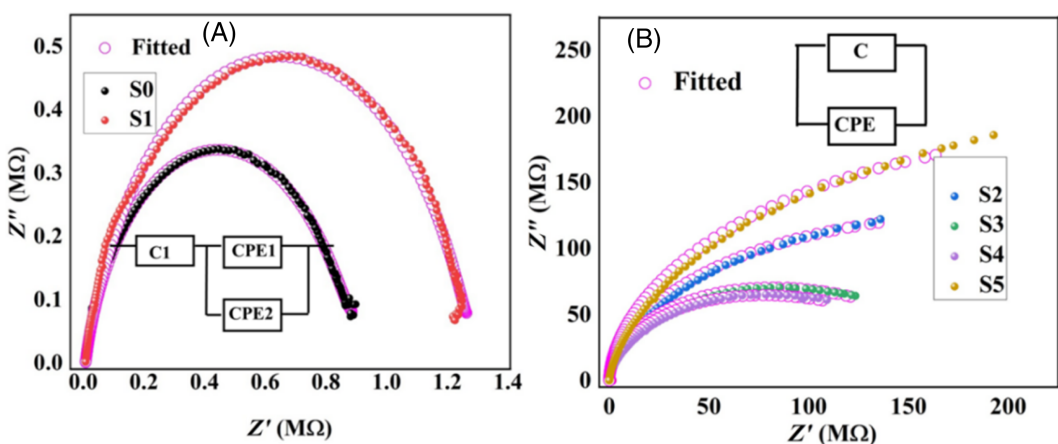


FIGURE 7 (A) The Nyquist plot and modified Cole–Cole fit of S0 and S1. (B) The Nyquist plot and modified Cole–Cole fit of neutron irradiated samples. CPE, constant phase element.

TABLE 5 Predicted values of capacitance (C) and constant phase element (CPE) as illustrated in Figure 6A,B based on the equivalent circuit model.

Samples	S0	S1	S2	S3	S4	S5
C (F/cm^2)	1.76×10^{-7} ± 15.40	1.28×10^{-7} ± 26.78	1.77×10^{-11} ± 0.77	1.83×10^{-11} ± 0.68	2.12×10^{-11} ± 0.81	1.46×10^{-11} ± 0.71
CPE1 ($\text{S}-\text{sn}/\text{cm}^2$)	1.05×10^{-6} ± 25.48	7.86×10^{-7} ± 0.21	1.57×10^{-9} ± 0.67	3.89×10^{-9} ± 0.51	4.03×10^{-9} ± 0.61	1.14×10^{-9} ± 0.77
n	0.012 ± 1.79	0.004 ± 8.53	0.21 ± 0.56	0.11 ± 0.83	0.12 ± 0.91	0.19 ± 0.69
CPE2 ($\text{S}-\text{sn}/\text{cm}^2$)	5.20×10^{-10} ± 0.400	3.21×10^{-10} ± 0.52	-	-	-	-
n	0.85 ± 0.050	0.83 ± 0.07	-	-	-	-

n = frequency factor.

GO and Ag NPs tend to increase the dielectric constant due to their conductive and polarizable nature, the cross-linking effect of GA tends to decrease the dielectric constant by restricting charge carrier mobility and enhancing crystallinity. The net effect observed in Figure 8A is a balance between these opposing influences, leading to an overall decline in the dielectric constant compared with pure PVA.

Upon irradiation, a reduction in ϵ' is observed across all irradiated samples. Neutron radiation deposits energy rapidly and randomly, creating localized energy states that activate long-lived excited sites and generate ions and free radicals. These ions and free radicals can subsequently cause molecule breakdown or cross-link formation. Additionally, hydrogen evolution during irradiation is also considered.⁹ These changes likely alter the polarizability of these composites.

As shown in Figure 2A, the disappearance of peaks at 1750–1650 cm^{-1} and the appearance of new peaks at 1450–1350 cm^{-1} indicate changes in the chemical structure of both NPs and the polymer matrix, leading to either cross-linking or chain scission. Cross-linking and chain scission can occur simultaneously, depending on the polymer's chemical structure, physical state, and irradiation conditions. In samples S2 and S3, cross-linking predominates restricting the mobility of polymer segments and hence disrupts dipole orientation, resulting in a diminished ϵ' . As the fluence increases to

$1.60 \times 10^{11} \text{ n}/\text{cm}^2$, cross-linking continues to predominate, reducing the disorder of dipolar groups and leading to an increase in ϵ' . However, further increasing the neutron fluence to $4.19 \times 10^{11} \text{ n}/\text{cm}^2$ (S5) results in a notable decrease in ϵ' magnitude. Higher fluencies may induce significant damage, including extensive chain scission and possibly further cross-linking forming a network structure that restricts the mobility of polymer segments, which can decrease the material's dielectric constant due to increased disorder and reduced charge carrier mobility. This decrease is attributed to the aggregation of NPs (as shown in Figure 1D), which diminishes the charge-storing capacity of the polymer NC.

The dielectric loss (ϵ'') (Figure 8B) decreases for S1 after the incorporation of fillers. Additionally, dielectric loss experiences a substantial decrease in irradiated samples, aligning with the trend observed in ϵ' . This observation implies that materials with lower conductivity typically demonstrate decreased dielectric constants and losses. Consequently, lower dielectric loss signifies less heat generation, reinforcing the potential effect of neutron irradiation on the electrical properties of the polymer NC.

Figure 8C illustrates the $\tan\delta$ variation with frequency for both unirradiated and irradiated samples. In the unirradiated state, S1 exhibits a higher $\tan\delta$ compared with S0. Following neutron

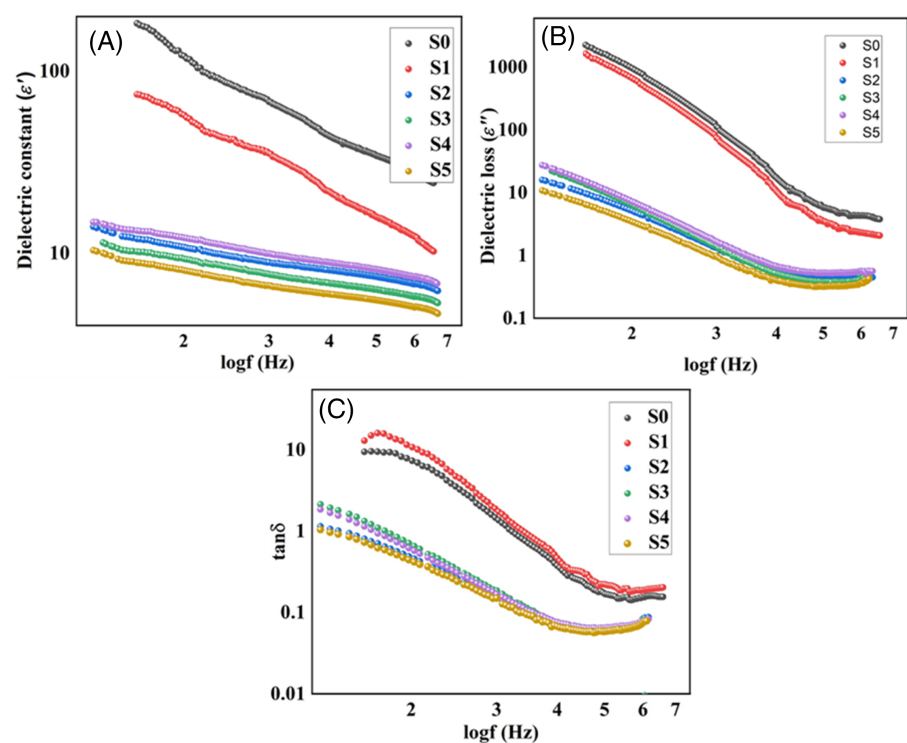


FIGURE 8 Dielectric properties of S0, S1, and neutron irradiated S2, S3, S4, and S5 polymer nanocomposites. (A) Plot of dielectric constant versus frequency of S0, S1, S2, S3, S4, and S5. (B) Illustrates the variation of dielectric loss with frequency of S0, S1, S2, S3, S4, and S5. (C) Depicts the variation of $\tan\delta$ with frequency of S0, S1, S2, S3, S4, and S5.

irradiation, the $\tan\delta$ value decreases, possibly indicating a shift of its peak to a lower frequency region with increasing neutron fluence. This behavior suggests that the NC sample operates as a system wherein one phase relaxes similarly to the amorphous phase, while the presence of a crystalline phase hinders the overall long-range segmental motions within the amorphous phase.⁴²

Abdelmalik's study reported that the impedance of neutron-irradiated epoxy TiO_2 samples ranged from 1×10^5 to 2.5×10^5 ohms.¹⁷ In contrast, the impedance in our current work varied significantly higher, from 80×10^6 to 123×10^6 ohms. This indicates that our PVA/GO-Ag/GA NCs exhibit much higher impedance under neutron irradiation compared with epoxy TiO_2 . Abdelmalik et al.'s¹⁸ another work reports that the dielectric constant of epoxy TiO_2 ranged from 7 to 14, while in our present work, the dielectric constant ranges from 10 to 15. Furthermore, the tangent loss for epoxy TiO_2 was reported to be between 0.5 and 0.7, whereas our study shows a tangent loss ranging from 0.9 to 2.5. These results demonstrate that PVA/GO-Ag/GA NCs under neutron irradiation possess higher impedance and slight enhanced dielectric properties compared with epoxy TiO_2 .

The changes in dielectric properties and impedance under neutron irradiation open up various potential applications, including energy storage applications, development of sensors for detecting radiation levels in various environments.

3.5.3 | ac conductivity studies

As shown in Figure 9A, the conductivity of S1 exhibits a consistent decrease across the entire frequency range. This decline could be

attributed to the reduced mobility of charge carriers, resulting from the scattering of ionized molecular aggregates, potentially formed due to the inhomogeneous distribution and non-bonding segments within the NC. In general, conductivity for all samples monotonically increases with rising frequency, indicating a conduction mechanism based on the hopping mechanism.⁴³ Moreover, upon irradiation, conductivity decreases for nearly all fluence levels considered in the investigation, as observed in Table 6 and depicted in Figure 9A, when compared with the unirradiated sample.

The Equation (5) highlights the dc conductivity values, as well as the fitting parameters A and s, which are essential for comprehending the electrical characteristics of the amorphous materials under investigation.⁴⁴

$$\sigma(\omega) = \sigma_{dc} + A\omega^s, \quad (5)$$

where A is a complex constant and the index s is the exponent of the angular frequency (ω). The trend in the dc conductivity values, along with the corresponding fitting parameters A and s, is indicative of the material's response to fast neutron irradiation. The observed decrease in s with increasing neutron fluence up to $1.04 \times 10^{10} \text{ n/cm}^2$ (S3), followed by an increase with higher fluence values. As depicted in Figure 9B, the linear slopes of $\sigma(\omega)$ versus ω provide insights into the exponent s and its variation with different conditions.

Moreover, the consistently maintained $s < 1$, except for S5, highlights the unique nature of the electrical conduction mechanism. The association between the frequency dependence of ac conductivity, the linearity of the response, and the irradiation-dependent s further

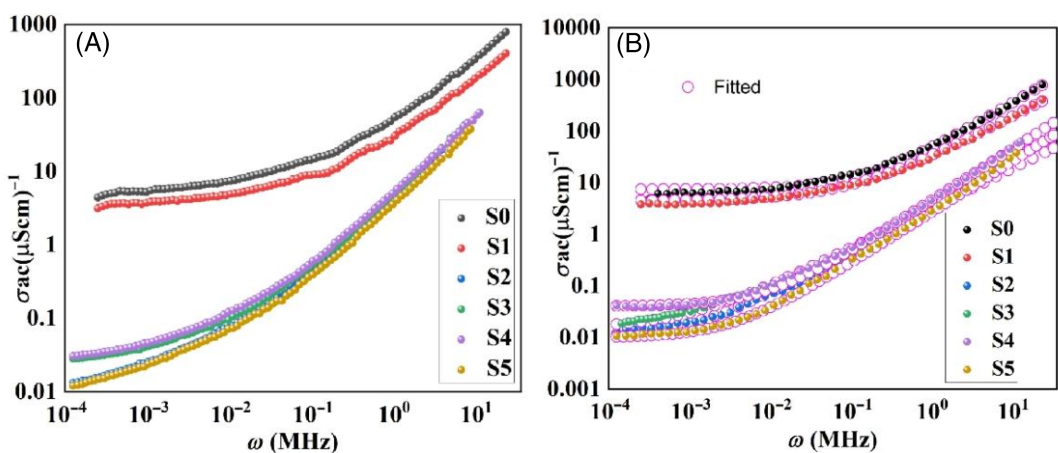


FIGURE 9 (A) Illustration of frequency-dependent ac conductivity of S0, S1, S2, S3, S4, and S5 polymer nanocomposites. (B) Demonstrates the application of Jonscher's fit to the frequency-dependent ac conductivity of S0, S1, S2, S3, S4, and S5.

TABLE 6 The dc conductivity values, along with the fitting parameters A and s from Jonscher's equation, $\sigma(\omega) = \sigma_{dc} + A\omega^s$ provide a comprehensive understanding of the electrical conduction characteristics, offering enhanced insights into the material's electrical behavior.

Samples	σ_{dc} Scm^{-1}	A	s
S0	$73.9 \times 10^{-7} \pm 0$	$1.28 \times 10^{-10} \pm 2.66 \times 10^{-13}$	0.92 ± 0
S1	$44.6 \times 10^{-7} \pm 0$	$4.58 \times 10^{-10} \pm 1.84 \times 10^{-12}$	0.80 ± 0
S2	$0.09 \times 10^{-7} \pm 1.73 \times 10^{-6}$	$1.93 \times 10^{-11} \pm 0$	0.9 ± 0
S3	$0.15 \times 10^{-7} \pm 0$	$7.04 \times 10^{-11} \pm 0$	$0.78 \pm 1.81 \times 10^3$
S4	$0.4 \times 10^{-7} \pm 2.27 \times 10^{-6}$	$4.56 \times 10^{-12} \pm 0$	1 ± 0
S5	$0.095 \times 10^{-7} \pm 4.99 \times 10^{-6}$	$8.05 \times 10^{-12} \pm 0$	0.94 ± 0

supports the applicability of the correlated barrier hopping (CBH) model.⁴⁵ These findings underscore the influence of neutron irradiation on the polymer matrix and its consequential impact on electrical transport properties, providing valuable insights for materials science and engineering applications. The shifts in α and β values correlate with changes in the NC's electrical properties. Increased heterogeneity and asymmetry in relaxation dynamics suggest that the material's dielectric constant and loss tangent are affected, impacting its overall dielectric performance. Neutron-induced defects and cross-linking hinder charge mobility, led to degraded electrical properties.

3.5.4 | Electric modulus study

The modulus formalism has been employed to explore the relaxation mechanism, utilizing the complex electric modulus (M^*). This method provides several advantages, particularly in its capacity to differentiate between electrode polarization and grain boundary conduction mechanisms. A notable advantage of using the electric modulus is its ability to mitigate electrode effects.⁴⁶ The complex electric modulus formalism, denoted as M^* , has been applied to amplify the impact of grains with small resistance, as described by Equation (6).

$$M^* = \frac{1}{\gamma_{\epsilon''}} = \frac{1}{(\epsilon' - j\epsilon'')} = M' + jM'' \quad (6)$$

In Figure 10A, the frequency-dependent real part of the electric modulus (M') characteristics for both irradiated and unirradiated NCs is depicted. At lower frequencies, M' values are negligible for S0 and S1, suggesting a minimal capacitive response in these specimens. However, for S0 and S1 samples, M' values increase at higher frequencies, indicating a more prominent capacitive response. In contrast, irradiated samples show an increase in M' values at lower frequencies, suggesting the presence of electrode potential. The M' value saturates at a maximum level at higher frequencies. The continuous dispersion observed with increasing frequency may be attributed to the short-range mobility of charge carriers.

In Figure 10B, the frequency-dependent spectra of M'' at various neutron fluence are illustrated. The variation of M'' with frequency at different neutron fluence provides valuable information about charge transport mechanisms, encompassing electrical transport and conductivity relaxation processes. The lower frequency region before the peak maximum of M'' represents the frequency range associated with charge carriers' mobility through a long-range hopping mechanism, while the higher frequency region after the peak denotes a range where charge carriers are constrained to short-range distances. The peak's frequency region indicates the transition in carriers' mobility from long to short range. The widening of the M'' peak signifies the real dielectric relaxation process and indicates the range of the relaxation time constant. Peaks in the frequency spectra of M'' across all samples suggest the presence of a conductivity relaxation process. However, for all irradiated samples the peak

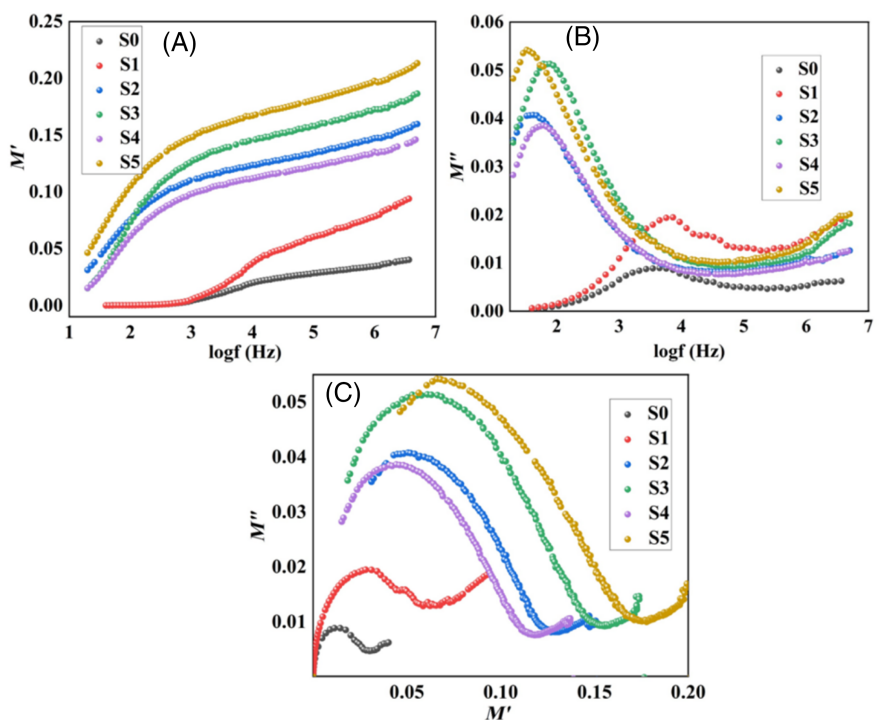


FIGURE 10 (A) The variation of the real part (M') of the electric modulus with the frequency of S0, S1, S2, S3, S4, and S5. (B) The frequency dependence of the imaginary part (M'') of the electric modulus under various neutron fluence conditions. (C) The plot of imaginary and real moduli of S0, S1, S2, S3, S4, and S5.

shifts to a lower frequency range indicating decrease in mobility or an increase in relaxation time. Among the irradiated samples, peak of S2 and S3 shifts to lower frequency range, but for S4 peak shifts to higher frequency range. Further increase in the irradiation fluence (S5) shifts the peak towards lower frequency range. This shift in the peak is as a result of irradiation-induced structural changes in the polymer matrix, such as cross-linking or scission. Cross-linking can constrain the movement of polymer chains and reduce the free volume available for charge transport, typically resulting in longer relaxation times and peak shifts to lower frequencies. On the other hand, chain scission can create more free volume and facilitate easier movement of charge carriers, shifting peaks to higher frequencies. Compared with unirradiated PVA/GO-Ag/GA NC, M'' increases in neutron-irradiated samples, suggesting decrease in dielectric constant (Equation 6).

Figure 10C, illustrates the variation of imaginary moduli with real moduli for both irradiated and non-irradiated films. Figure 10C, the correlation plot of M' versus M'' for S0 and S1 illustrates an increase in M'' corresponding to an elevation in M' , culminating in a discernible peak at higher frequencies. Notably, this peak undergoes a shift towards a lower frequency region in the case of the neutron-irradiated sample. This observed shift in the peak frequency provides valuable information about the altered charge transport dynamics induced by neutron irradiation. However, for the present system, the (M' and M'') peaks do not overlap suggesting the components form long-range relaxation.²⁰

4 | CONCLUSION

PVA/GO-Ag/GA polymer NCs became opaque to UV light, with a reduction in transmittance to 78% after neutron irradiation,

suggesting they are highly suitable for deployment in UV shielding coatings or packaging materials. The energy band gap decreased from 5.25 to 4.09 eV upon irradiation, which brings about the possibility of tailoring the band gap for the potential utility of these films in electronic and optoelectronic applications. Upon neutron irradiation, PVA/GO-Ag/GA polymer NCs exhibit increased relaxation time from 7.63×10^{-4} to 0.02 s, a decrease in conductivity from 44.6×10^{-7} to 0.09×10^{-7} S/cm, an increase in impedance, and a decrease in dielectric loss, cautioning us that these composites are vulnerable to neutron exposure with regard to their power density when employed for energy storage purposes. The investigation of frequency-dependent M' and M'' parts of the electric modulus in PVA and PVA/GO-Ag/GA NCs reveals distinct capacitive responses, altered conductivity relaxation processes, and a noteworthy shift in peak frequency in neutron-irradiated samples. Further investigation might aim to deepen the understanding of how neutron irradiation affects the thermal and mechanical properties. By combining experimental studies with simulation, and comparative analyses, one can develop a comprehensive understanding of the irradiation effects, leading to the development of materials with improved performance.

ACKNOWLEDGMENTS

The authors are thankful to the Director of Manipal Centre for Natural Sciences, Manipal Academy of Higher Education, Manipal 576104, Karnataka, India.

FUNDING INFORMATION

This research did not receive any specific grant from funding agencies in the public, commercial, or not-for-profit sectors.

CONFLICT OF INTEREST STATEMENT

The authors declare no conflict of interest.

DATA AVAILABILITY STATEMENT

Data Availability Statement: The authors declare that the data supporting the findings of this study are available within the paper.

ORCID

K. M. Eshwarappa  <https://orcid.org/0000-0002-7850-4490>

REFERENCES

1. Miroshnichenko LI. *Radiation Hazard in Space*. Springer; 2003. doi:[10.1007/978-94-017-0301-7](https://doi.org/10.1007/978-94-017-0301-7)
2. Mruthyunjayappa KC, Paramashivaiah SA, Mallikarjunappa EK, et al. A combined experimental and computational study of flexible polyvinyl alcohol (PVA)/graphene oxide (GO) nanocomposite films for superior UV shielding with improved mechanical properties. *Mater Today Commun*. 2023;35:105662. doi:[10.1016/j.mtcomm.2023.105662](https://doi.org/10.1016/j.mtcomm.2023.105662)
3. Muhammed AA, Zgair IA, Hussein MA, Mahdi LH, Jabbar BS, Alkhayatt AHO. Preparation and optical characterizations of PVA: Ag nano composite. *J Phys Conf Ser*. 2021;1879:032083. doi:[10.1088/1742-6596/1879/3/032083](https://doi.org/10.1088/1742-6596/1879/3/032083)
4. Khairy M, Gouda ME. Electrical and optical properties of nickel ferrite/polyaniline nanocomposite. *J Adv Res*. 2015;6:555-562. doi:[10.1016/j.jare.2014.01.009](https://doi.org/10.1016/j.jare.2014.01.009)
5. Selvi J, Mahalakshmi S, Parthasarathy V, et al. Optical, thermal, mechanical properties, and non-isothermal degradation kinetic studies on PVA/CuO nanocomposites. *Polym Compos*. 2019;40:3737-3748. doi:[10.1002/pc.25235](https://doi.org/10.1002/pc.25235)
6. Sun X, Huang C, Wang L, et al. Recent progress in graphene/polymer nanocomposites. *Adv Mater*. 2021;33:e2001105. doi:[10.1002/adma.202001105](https://doi.org/10.1002/adma.202001105)
7. Slowinski B, Adawi A. *Changes of Properties of Selected Glasses Irradiated with Gamma Rays and Neutrons: A Short Overview*. Vacuum. Vol 63; 2001:585-589.
8. Basha AF, Basha MAF. Impact of neutron irradiation on the structural and optical properties of PVP/gelatin blends doped with dysprosium (III) chloride. *J Appl Phys*. 2017;122:235104. doi:[10.1063/1.5008494](https://doi.org/10.1063/1.5008494)
9. Prasher S, Kumar M. Effects of neutron irradiation on polymer. In: Kumar V, Chaudhary B, Sharma V, Verma K, eds. *Radiation Effects in Polymeric Materials*. Springer; 2019:351-368. doi:[10.1007/978-3-030-05770-1_11](https://doi.org/10.1007/978-3-030-05770-1_11)
10. Zirkle RE, Aebersold PC. Relative effectiveness of x-rays and fast neutrons in retarding growth. *Proc Natl Acad Sci*. 1936;22:134-138. doi:[10.1073/pnas.22.2.134](https://doi.org/10.1073/pnas.22.2.134)
11. Was GS. *Fundamentals of Radiation Materials Science: Metals and Alloys*. 2nd ed. Springer; 2016. doi:[10.1007/978-1-4939-3438-6](https://doi.org/10.1007/978-1-4939-3438-6)
12. Baranov V, Davydov YI, Erasmus R, et al. Effects of neutron radiation on the optical and structural properties of blue and green emitting plastic scintillators. *Nucl Inst Methods Phys Res B*. 2018;436:236-243. doi:[10.1016/j.nimb.2018.10.002](https://doi.org/10.1016/j.nimb.2018.10.002)
13. Mallick B, Chandra Behera R, Panigrahi S, et al. Microstructural analysis of neutron-irradiation induced changes in polyester fibre studied using EPMA. *Indian J Phys*. 2009;83:525-529.
14. Rafik H, Izerrouken M. Radiation damage induced by reactor neutrons in nano-anatase TiO₂ thin film. *Radiat Phys Chem*. 2020;177:109114. doi:[10.1016/j.radphyschem.2020.109114](https://doi.org/10.1016/j.radphyschem.2020.109114)
15. Chikaoui K, Izerrouken M, Djebbara M, Abdesselam M. Polyethylene terephthalate degradation under reactor neutron irradiation. *Radiat Phys Chem*. 2017;130:431-435. doi:[10.1016/j.radphyschem.2016.10.002](https://doi.org/10.1016/j.radphyschem.2016.10.002)
16. Sinha E, Rout SK. Effect of neutron irradiation on the structural, mechanical, and thermal properties of jute fiber. *J Appl Polym Sci*. 2008;110:413-423. doi:[10.1002/app.28504](https://doi.org/10.1002/app.28504)
17. Abdelmalik AA, Abubakar YM, Ogbodo MO, Victor KY, Goje HG. Effect of neutron irradiation on the impedance of epoxy-TiO₂ nanocomposite for electric power insulation. *Radiat Phys Chem*. 2021;179:109215. doi:[10.1016/j.radphyschem.2020.109215](https://doi.org/10.1016/j.radphyschem.2020.109215)
18. Abdelmalik AA, Ogbodo MO, Abubakar YM, Galadima AI, Aliyu A, Jonah SA. Influence of neutron irradiation on the mechanical and dielectric properties of epoxy/ titanium oxide nanocomposite. *Radiat Phys Chem*. 2022;198:110230. doi:[10.1016/j.radphyschem.2022.110230](https://doi.org/10.1016/j.radphyschem.2022.110230)
19. Shilpa MP, Cyriac V, Gurumurthy SC, Ismayil S, Shet KV, Subbaiah MSM. A novel approach to enhance the ionic conductivity of silver nanoparticles incorporated PVA:NaBr polymer electrolyte films via fast neutron irradiation. *Radiat Phys Chem*. 2024;218:111590. doi:[10.1016/j.radphyschem.2024.111590](https://doi.org/10.1016/j.radphyschem.2024.111590)
20. Yang G, Cui J, Ohki Y, Wang D, Li Y, Tao K. Dielectric and relaxation properties of composites of epoxy resin and hyperbranched-polyester-treated nanosilica. *RSC Adv*. 2018;8:30669-30677. doi:[10.1039/C8RA05846F](https://doi.org/10.1039/C8RA05846F)
21. Abuali Galehdari N, Kelkar AD. Effect of neutron radiation on the mechanical and thermophysical properties of nanoengineered polymer composites. *J Mater Res*. 2017;32:426-434. doi:[10.1557/jmr.2016.494](https://doi.org/10.1557/jmr.2016.494)
22. Canel A, Korkut H, Korkut T. Improving neutron and gamma flexible shielding by adding medium-heavy metal powder to epoxy based composite materials. *Radiat Phys Chem*. 2019;158:13-16. doi:[10.1016/j.radphyschem.2019.01.005](https://doi.org/10.1016/j.radphyschem.2019.01.005)
23. Jiao L, Wang Y, Wu Z, et al. Effect of gamma and neutron irradiation on properties of boron nitride/epoxy resin composites. *Polym Degrad Stab*. 2021;190:109643. doi:[10.1016/j.polymdegradstab.2021.109643](https://doi.org/10.1016/j.polymdegradstab.2021.109643)
24. Behmanesh B, Rezaei-Ochbelagh D, Azizian-Kalandaragh Y, Imanzadeh-Karkaragh G. Sonochemical preparation of Ag2O-PVA nanocomposites: study on pertinent structural and optical properties and exploring the effect of gamma and neutron irradiation. *Curr Sci*. 2017;112:735-742. doi:[10.18520/cs/v112/i04/735-742](https://doi.org/10.18520/cs/v112/i04/735-742)
25. Kavitha CM, Eshwarappa KM, Shetty SJ, et al. Modification of thermal and electrical characteristics of hybrid polymer nanocomposites through gamma irradiation for advanced applications, discover. *Nano*. 2024;19:34. doi:[10.1186/s11671-024-03972-3](https://doi.org/10.1186/s11671-024-03972-3)
26. Farag OF. Comparison of the effect of plasma treatment and gamma ray irradiation on PS-Cu nanocomposite films surface. *Results Phys*. 2018;9:91-99. doi:[10.1016/j.rinp.2018.02.031](https://doi.org/10.1016/j.rinp.2018.02.031)
27. Kavitha CM, Eshwarappa KM, Gurumurthy SC, Karunakara N, Mallikarjun I. Gamma radiation-induced modification in mechanical properties of hybrid PVA (Go/Ag)-based polymer nanocomposites. *Arab J Sci Eng*. 2024;49:1-10. doi:[10.1007/s13369-024-08964-0](https://doi.org/10.1007/s13369-024-08964-0)
28. Stevens MP. *Polymer Chemistry: An Introduction*. 3rd ed. Oxford University Press; 1999.
29. Silverstein RM, Webster FX, Kiemle DJ, Bryce DL. *Spectroscopic Identification of Organic Compounds*. 8th ed. Wiley; 2023.
30. Rudra R, Kumar V, Kundu PP. Acid catalysed cross-linking of poly vinyl alcohol (PVA) by glutaraldehyde: effect of crosslink density on the characteristics of PVA membranes used in single chambered microbial fuel cells. *RSC Adv*. 2015;5:83436-83447. doi:[10.1039/c5ra16068e](https://doi.org/10.1039/c5ra16068e)
31. Kavitha CM, Eshwarappa KM, Shilpa MP, et al. Tuning the optical and electrical properties by gamma irradiation of silver nanoparticles decorated graphene oxide on glutaraldehyde crosslinked polyvinyl alcohol matrix. *Mater Res Bull*. 2024;173:112685. doi:[10.1016/j.materresbull.2024.112685](https://doi.org/10.1016/j.materresbull.2024.112685)
32. Abdelghany AM, Abdelrazeq EM, Badr SI, Morsi MA. Effect of gamma-irradiation on (PEO/PVP)/Au nanocomposite: materials for electrochemical and optical applications. *Mater Des*. 2016;97:532-543. doi:[10.1016/j.matdes.2016.02.082](https://doi.org/10.1016/j.matdes.2016.02.082)
33. Sharma N, Tomar S, Shkir M, Choubey RK, Singh A. Study of optical and electrical properties of graphene oxide. *Mater Today Proc*. 2021;36:730-735. doi:[10.1016/j.matpr.2020.04.861](https://doi.org/10.1016/j.matpr.2020.04.861)

34. Kareem AA, Polu AR, Rasheed HK, Alomayri T. Effect of silver nanoparticles on structural, thermal, electrical, and mechanical properties of poly(vinyl alcohol) polymer nanocomposites. *Polym Compos*. 2023; 44:3281-3287. doi:[10.1002/pc.27319](https://doi.org/10.1002/pc.27319)
35. Nafee SS, Hamdalla TA. Effect of neutron irradiation on the optical properties of PMMA/RhB used in optical fiber amplification. *J Radioanal Nucl Chem*. 2019;320:101-108. doi:[10.1007/s10967-019-06440-w](https://doi.org/10.1007/s10967-019-06440-w)
36. Lin PB. *Ceramic Materials Research Trends*. Nova Science Publishers; 2007.
37. Lvovich VF. *Impedance Spectroscopy: Applications to Electrochemical and Dielectric Phenomena*. John Wiley & Sons, Inc; 2012. doi:[10.1002/9781118164075](https://doi.org/10.1002/9781118164075)
38. Barsoukov E, Macdonald JR. *Impedance Spectroscopy: Theory, Experiment, and Applications*. John Wiley & Sons; 2005. doi:[10.1002/0471716243](https://doi.org/10.1002/0471716243)
39. Kremer F, Schönhals A, eds. *Broadband Dielectric Spectroscopy*. Springer; 2003. doi:[10.1007/978-3-642-56120-7](https://doi.org/10.1007/978-3-642-56120-7)
40. Gateman SM, Gharbi O, Gomes de Melo H, Ngo K, Turmine M, Vivier V. On the use of a constant phase element (CPE) in electrochemistry. *Curr Opin Electrochem*. 2022;36:101133. doi:[10.1016/j.coelec.2022.101133](https://doi.org/10.1016/j.coelec.2022.101133)
41. Abutalib MM, Guirguis OW. Fast neutrons effect on the frequency-dependent dielectric properties of PVA/HPC blend. *Mater Sci*. 2014; 10:391-396.
42. abo-Ellil MS, Gaafer SA, El-Kader FHA, Kamel NA. Effect of fast neutrons on dielectric properties of pure and gelatin doped-poly (vinyl alcohol) films. *J Polym Res*. 2000;7:149-153. doi:[10.1007/s10965-006-0114-z](https://doi.org/10.1007/s10965-006-0114-z)
43. Aziz SB, Marf AS, Dannoun EMA, Brza MA, Abdullah RM. The study of the degree of crystallinity, electrical equivalent circuit, and dielectric properties of polyvinyl alcohol (PVA)-based biopolymer electrolytes. *Polymers (Basel)*. 2020;12:1-17. doi:[10.3390/polym12102184](https://doi.org/10.3390/polym12102184)
44. Gogoi P, Srinivas P, Sharma P, Pamu D. Optical, dielectric characterization and impedance spectroscopy of Ni-substituted MgTiO₃ thin films. *J Electron Mater*. 2016;45:899-909. doi:[10.1007/s11664-015-4209-3](https://doi.org/10.1007/s11664-015-4209-3)
45. Dutta P, Biswas S, Ghosh M, De SK, Chatterjee S. The dc and ac conductivity of polyaniline–polyvinyl alcohol blends. *Synth Met*. 2001; 122:455-461. doi:[10.1016/S0379-6779\(00\)00588-9](https://doi.org/10.1016/S0379-6779(00)00588-9)
46. Jung W-H. Dielectric relaxation and hopping conduction in La₂NiO_{4+δ}. *J Mater*. 2013;2013:1-6. doi:[10.1155/2013/169528](https://doi.org/10.1155/2013/169528)

How to cite this article: Kavitha CM, Eshwarappa KM, Shilpa MP, et al. Hybrid polymer nanocomposites with tailored band gaps and UV absorption for advanced applications in optoelectronics and UV protection. *Polym Adv Technol*. 2024; 35(7):e6515. doi:[10.1002/pat.6515](https://doi.org/10.1002/pat.6515)